Conformational and Packing Modeling of Optically Active Polyesters. 1. Planar Zigzag Structure of Isotactic Polylactone

Ziru He, Josée Brisson, and Robert E. Prud'homme*

Département de chimie, Centre de recherche en sciences et ingénierie des macromolécules, Faculté des Sciences et de Génie, Université Laval, Sainte-Foy, Québec, Canada G1K 7P4

Received May 26, 1998; Revised Manuscript Received September 8, 1998

ABSTRACT: The optically active and crystalline poly(α-methyl-α-ethyl-β-propiolactone) (PMEPL) shows conformational changes and polymorphic behavior depending on the preparation method of the sample. The melt-crystallized isotactic PMEPL exhibits a monoclinic lattice and an extended planar zigzag conformation. Using computational modeling, we have solved and refined its crystal structure. Both the two-step and single-step procedures were used to evaluate packing energies. The results indicate that two chains with the same chirality and opposite directions pass through a monoclinic unit cell having lattice dimensions $a = 9.10$, $b = 7.44$, c(fiber period) $= 4.84$ Å and $\beta = 83.1°$. The space group is $P2_1$ with unique axis b. The final crystal structure was confirmed by comparison with electron diffraction data and X-ray powder diffraction spectra. Both procedures result in crystal structures in good agreement with the experiments. The final discrepancy R factors are 0.16 for the flexible model and 0.20 for the rigid model when compared to X-ray data and 0.20 for the flexible model and 0.23 for the rigid model when compared to electron diffraction data.

Introduction

The combination of molecular modeling with diffraction experiments provides a powerful tool for resolving and refining the crystal structure of a polymer. Energy calculations made for single molecules and crystals may serve three purposes:[1] (1) they clarify the factors governing the crystal and molecular structure already determined experimentally; (2) they allow us to predict the most stable molecular conformation and its crystal packing starting from the chemical structure; and (3) they provide a collection of reliable potential functions and parameters for intra- and intermolecular interactions based on well-defined crystal structures. During the refinement of a crystal structure, the computational accuracy depends not only on the quality of the semiempirical force field used but also on the choice of the starting conformation, on the chain position in the unit cell, and on the correct molecular symmetry.

The traditional determination of the molecular packing in crystals uses two approaches, i.e., the two-step[2,3] and single-step[4−7] procedures. In the former case, the conformation of the polymer chain is first built and minimized while taking into account only the intramolecular (bonded and nonbonded) energy contributions and, subsequently, a rigid-body refinement is performed in the unit cell by translating and rotating the chains to minimize intermolecular interactions. The conformations having a minimum energy and agreeing with experimental data (such as torsion angles based on chemical shifts in the ^{13}C solid-state NMR spectroscopy of fibers and as derived from the repeat period measured by X-ray diffraction) are used as starting points in building crystal structures. The basic underlying assumptions of this approach are that intra- and intermolecular interactions can be considered independently[8] and that the depth of the intramolecular potential energy minima is much more pronounced than that pertaining to minima of packing energy.[6] This approximation has been proved valid, especially when the starting conformation is very close to the real situation.

However, when the starting conformation deviates greatly from the real one, or when several conformations of comparable energy have to be discriminated, the two-step procedure may be significantly biased.[6,7] For example, the intermolecular packing energy may cause the minimum-energy conformation for a helix within a polymer crystal not to correspond to the minimum-energy conformation for the free chain. In this case, a more accurate calculation is required. The single-step approach was thus developed to take into account both intra- and intermolecular interactions simultaneously. Not only are the packing and cell parameters allowed to vary, but also the internal geometry can be relaxed.[9] This method has been used successfully for the refinement of the crystal structures of a few polyesters,[5,6] including α- and γ-polypivalolactones (PPLs).[6]

Poly(α-methyl-α-ethyl-β-propiolactone) (PMEPL) is similar to PPL, but the substitution of a methyl group by an ethyl side chain leads to the chirality of the repeat unit. Subsequently, the isotactic polymer, which has the same absolute configuration for all chiral carbon atoms, is optically active. There are several reasons for studying the crystal structures of optically active PMEPL. First of all, PMEPL shows conformational changes and polymorphic behavior depending on the preparation method of the sample.[10−13] The melt-crystallized isotactic PMEPL exhibits a monoclinic, pseudo-orthorhombic lattice with a unit cell parameter c (4.75 Å) equal to the periodicity of the planar zigzag conformation whereas solution-cast isotactic films and atactic samples give distinctly different orthorhombic lattice dimensions where the chains are in a 2_1 helical conformation with a fiber period of about 5.8 Å. The conformation of these

* To whom correspondence should be addressed.

10.1021/ma980830l CCC: $15.00
Published on Web 10/28/1998

polymorphs was partly derived in previous studies using spectroscopic (infrared and solid-state NMR) and diffraction methods (X-ray powder and electron diffraction).[10−13] Second, the mixture of two isotactic PMEPL samples of opposite configuration with a 1:1 statistical ratio yields polymorphs. This stereocomplex crystallizes in an orthorhombic lattice with a 2_1 helical conformation. The fiber period of the stereocomplex is significantly longer (∼7.1 Å) than that of isotactic PMEPL.

In this article, we will consider the refinement of the isotactic PMEPL crystal structure prepared from the melt, the exact structure and the packing symmetry of which have never been investigated before. An energy analysis of the isolated chain will first be performed, and then, reasonable chain conformations and internal geometry will be used to build the crystal structure. The final crystal structures, minimized from both the rigid and flexible approaches, will be compared and quantitatively refined using electron diffraction data, X-ray powder diffraction spectra and structure factor calculation.

Methods of Calculation

A single chain was built to perform the analysis of both conformational energies and geometry. Conformations with minimum energies and suitable internal geometries were preferentially considered as starting conformations for chain packing. All calculations and simulations were based on the polymer consistent force field (PCFF),[9,14,15] an extension for polymers of the CFF91,[9,14,15] Insight II, and Discover simulation software (MSI),[9] and were carried out on a Silicon Graphics INDIGO II workstation. The total potential energy of a single chain included the contributions from each of the internal valence coordinates (bond stretching, bond angle bending, torsion, and Wilson out-of-plane), the cross-coupling terms between various internal coordinates (bond length, angle, and torsion), and nonbonded interactions (van der Waals and Coulombic). This force field employs a quadratic polynomial for bond stretching and angle bending and a three-term Fourier expansion for torsions. The Lennard-Jones 9−6 potential was used to evaluate the van der Waals interactions. The dipole moments of the ester, methyl, and methylene groups were decomposed into atomic partial charges, and the net atomic charge of each repeat unit was zero. The effective dielectric constant was chosen as 1. A cutoff limit of 10 Å was applied for the nonbonded interactions of both the isolated chain and the crystalline structure.

Isolated Chain. From previous work, it is known that the isotactic PMEPL can adopt two conformations in the crystalline state, that is, the planar zigzag and the 2_1 helix, depending on the thermal history of the sample. Melt-crystallized isotactic PMEPL exhibits an all-trans backbone conformation, but the side-chain conformation remains uncertain. Using computer simulation, we first built an all-atom model of the all-trans backbone conformation. In Figure 1a is shown the repeat unit used in the calculation with atomic numeration whereas Figure 1b illustrates the corresponding model compound with two repeat units. There are four dihedral angles (τ, ψ, η, and ϕ) along the backbone chain for each repeat unit, but each dihedral angle was constrained at 180°. The corresponding Fischer projection with two repeat units is also given on the right-hand side of the figure. In an ideal crystal, each asymmetric repeat unit should have the same atomic environment. Therefore, in this case, since the fiber period contains only one repeat unit, χ_1 must be equal to χ_2.

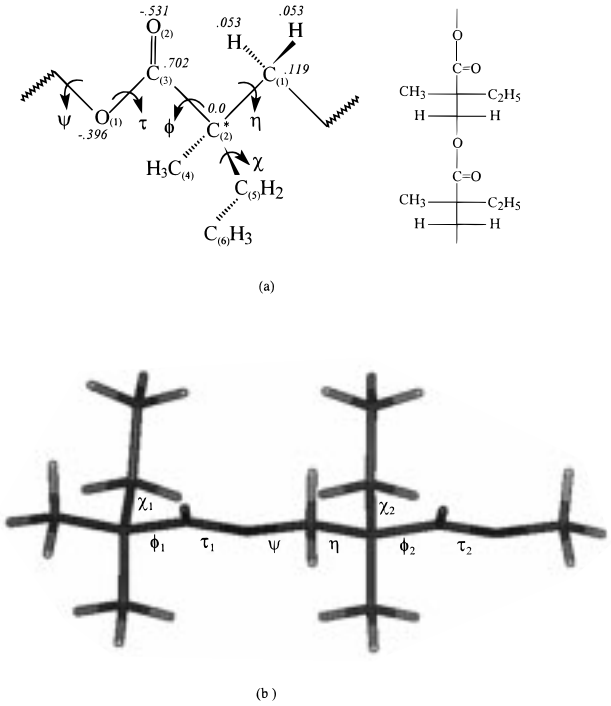

Figure 1. Model structures with their dihedral angles: (a) conformational repeat unit with *R* chirality, atomic partial charges, and Fischer projection; (b) model compound.

A full-relaxation optimization was then used to calculate the potential energies of the all-trans backbone model compound as a function of the side-chain orientations. The torsion angle χ was calculated using a grid of 5° in the range 0−360°. The group-based cutoff method[9] was employed for both the van der Waals and Coulombic potential summations of the isolated chain; that is, nonbonded interactions are included only if the distance between two given functional groups is shorter than the cutoff distance. Unlike the case for the cutoff distance based on atom−atom pairs, this method prevents artifacts due to splitting of dipoles. This minimizing strategy uses three different algorithms which are automatically changed from the steepest descent (RMS = 100) to the conjugate gradient of Polak-Ribiere (RMS = 1.0), followed by the BFGS Newton method (RMS = 0.001). The total iteration was limited to a maximum of 1000 steps, and convergence was reached in all cases.

Crystal Model Building and Refinement. Different packing forms for the $P2$ and $P2_1$ space groups were examined by both energy analysis and diffraction simulations. Energy calculations were performed using the same parameters as for the single chain, although an accurate calculation requires a proper simulation of thermal motion.[6] The atom-based cutoff method was used for the summation of nonbonded interactions. In a first step, a rigid-body rcfinement was performed by keeping the initial geometry (bond length, bond angle, and torsion angle) and unit cell parameters fixed, except for the monoclinic angle. The packing fractional position and the setting angle of the chains were varied until low energy and reasonable X-ray and electron diffraction patterns of the crystal structure were reached. The final crystal structure was established by flexible modeliza-

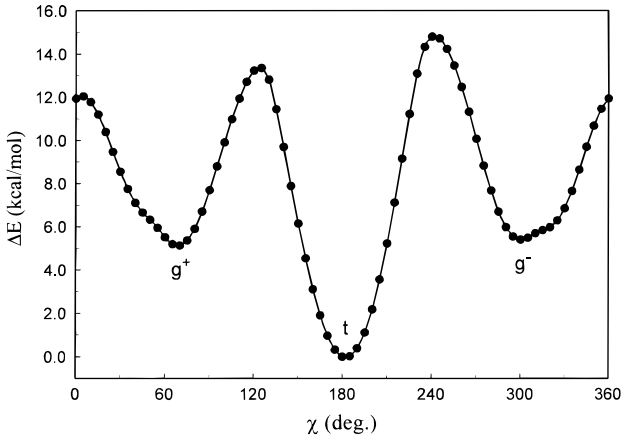

Figure 2. Potential energy curve of the planar zigzag backbone conformation as a function of the side-chain orientation as described by χ (see Figure 1). All data were normalized using the lowest energy (49.52 kcal/mol) of the trans side chain.

tion in which both intra- and intermolecular interactions are minimized simultaneously; the Cartesian coordinates of the chain repeat unit atoms and the monoclinic angle are thus varied while keeping fixed only the symmetry of the space group and the a, b, c, α, and γ parameters at the unit cell. In this way, the intramolecular geometry is varied along with the setting angle, the chain offset Z_2 along the c axis, and the xy position of the asymmetric unit in the cell. Finally, the two crystal structures optimized from the single-step and the two-step methods were refined quantitatively against electron diffraction data, X-ray powder diffraction intensities, and structure factor calculations.

X-ray and electron diffraction experiments are described elsewhere.[11] Measured structure factors (F_o)[1,16] for X-ray are equal to the square roots of the experimental diffraction intensities (I) corrected by $Lp = (1 + \cos^2 2\theta)/(\sin^2 \theta \cos \theta)$, that is, $F_o = [I/(KLp)]^{1/2}$, where K is a scaling factor. The intensity was evaluated by measuring the area of the peaks in the X-ray powder diffraction pattern,[10] after subtraction of the amorphous halo. Calculated structure factors (F_c) were computed as $F_c = (\sum_{i=1}^{n} m_i |F_i|^2)^{1/2}$, where m_i is the multiplicity factor and n is the total number of reflections contributing to a single peak in the powder spectrum.

The $hk0$ electron diffraction intensities were digitized from the originally positive and negative photographs by the SigmaScan image analysis v2.0 software (Jandel Scientific) and a microscope, and the background around each spot was removed. A visual estimation was used for the intensities of the $0kl$ electron diffraction pattern. Neither polarization corrections (unknown in electron diffraction) nor Lorentz corrections have been performed in this study, although quasi-Lorentz corrections could account for the effect of crystal geometry in diffraction intensity measurement.[17] The discrepancy factor R was calculated as $R = \sum|F_o - F_c|/\sum F_o$ for both X-ray and electron diffractions.

Results and Discussion

Conformational Energy Calculations. Conformational energies were evaluated as a function of the side-chain dihedral angle χ, on an all trans-backbone model compound, as shown in Figure 2. All energy data were normalized using the lowest calculated energy (49.52 kcal/mol) of the backbone conformation with the trans side chain. Among all-trans backbone conformations, the one with the trans side chain (0.0 kcal/mol) is energetically much more favored as compared to those with gauche side chains (5.13 kcal/mol for g^+ and 5.40 kcal/mol for g^-). Nevertheless, these three conformations were used as starting points for building PMEPL unit cells, considering various space groups, symmetries, and cell dimensions.

Chain Packing in Different Possible Space Groups. The electron diffraction data of both single crystals and epitaxial crystals[11] indicate that the two observed zero-level ($hk0$ and $0kl$) reciprocal planes show a 2 mm symmetry. The cell parameters, after calibrating the electron diffraction data, are $a = 9.10$, $b = 7.44$, $c = 4.75$ Å, and $\alpha = \gamma = 90°$. It was speculated that β is close to 90° on the basis of X-ray diffraction data of nonoriented samples. Analytically, if $\beta = 90°$, the possible crystal lattices are orthorhombic or monoclinic; if $\beta \neq 90°$, then a monoclinic lattice with a unique b axis is the only possibility that respects the observed symmetry.

It was determined previously[11] from density calculations that the unit cell contains two repeat units. For the PMEPL planar zigzag conformation, each repeat unit is an asymmetric repeat unit. Since PMEPL is a chiral molecule and all orthorhombic space groups have a minimum of four general positions and mirror or glide planes, it is impossible to place two repeat units in an orthorhombic lattice: the orthorhombic space groups must then be eliminated due to this symmetry consideration. It is therefore necessary to consider a monoclinic or, less probably, a triclinic space group.

For a monoclinic symmetry, the only space groups that agree with these restrictions are $P2$ and $P2_1$, in which the general position accommodates two repeat units. In these two space groups, the chain can be packed parallel or antiparallel, depending on the identity of the unique axis. If the two chains are packed parallel, the possible space group is $P2$ with a unique c axis or $P2_1$ with a unique c axis. On the other hand, if the two chains are packed antiparallel, the space group can then be $P2$ or $P2_1$ with a unique a or b axis.

After optimization, a set of low-energy packing forms were obtained for the selected space groups. All the corresponding packing densities were very close to the experimental value 1.10 g/cm^3. The $P2$ space group with a unique a or b axis was first excluded due to severe steric interferences between the two chains whatever the side-chain orientation, since several nonbonded atoms overlap and are located within the standard van der Waals distances. As a result, the packing energies are very high. In contrast, the $P2(c)$ and $P2_1(a,b,c)$ space groups are allowed from the energetic point of view (note that the a, b, and c symbols in parentheses are the unique axes corresponding to the specific space group mentioned). As mentioned above, $P2_1(b)$ meets the condition of the 2 mm symmetry for the $hk0$ and $0kl$ projections in electron diffraction patterns whether β is 90° or not; it is then a good candidate for further calculations using three side-chain models (trans, g^+, and g^-). $P2(c)$ and $P2_1(a,c)$ are also possible when the α and γ angles are equal to or very close to 90°. These space groups were also considered because of possible slight deviations from symmetry not detected by electron diffraction. To select the best model, the electron diffraction patterns of single crystals and the X-ray powder diffraction profiles were simulated

Table 1. Comparison of Calculated and Observed Relative Intensities of the X-ray Powder Diffraction Pattern for Various Packing Symmetries and Side-Chain Conformations[a]

Miller indices *hkl*	obsd intensity I_o	calc relative intensities											
		trans				g^+				g^-			
		P2(*c*)	P2$_1$(*a*)	P2$_1$(*b*)	P2$_1$(*c*)	P2(*c*)	P2$_1$(*a*)	P2$_1$(*b*)	P2$_1$(*c*)	P2(*c*)	P2$_1$(*a*)	P2$_1$(*b*)	P2$_1$(*c*)
100	27.0 (s)	s	*a*	s	s	m	*a*	s	vw	m	*a*	s	m
110	100 (vs)	vs	vs	vs	vs	vs	vs	vs	vs	vs	vs	vs	vs
200	8.4 (m)	m	s	m	m	s	m	vw	s	s	vw	vw	s
$10\bar{1}$[b]	9.6 (m)	m	m	ms	ms	ms	m	w	w	m	vw	w	w
210	12.5 (ms)	m	a	ms	m	m	a	ms	vw	vw	m	m	m
020	9.7 (m)	ms	s	m	ms	w	w	m	ms	m	m	m	w
120	16.2 (ms)	s	a	ms	ms	ms	m	s	ms	ms	vw	s	m
201	(w)	w	a	w	m	w	ms	w	w	w	vw	w	m
001	(a)	ms	a	a	a	m	a	w	w	s	m	a	m
101	(a)	w	a	a	ms	a	a	a	w	a	a	a	a
010	(a)	a	a	a	a	m	a	a	m	a	w	a	a

[a] vs = very strong; s = strong; ms = medium strong; m = medium; w = weak; vw = very weak; a = absent. [b] Previously indexed as 011 in the orthorhombic unit cell.

for all crystal structures produced from the different space groups. A qualitative comparison between the observed X-ray powder diffraction diagram and the calculated X-ray diagram for the different models (space group and side-chain conformations) is given in Table 1.

Experimentally, the electron diffraction pattern of the melt-crystallized isotactic PMEPL[11] exhibits a 2 mm symmetry for both the *hk*0 reciprocal lattice of the single crystal and the 0*kl* lattice of the epitaxially crystallized sample. Only the $P2_1(b)$ space group is compatible with the observed symmetry. For the $P2_1(a)$ space group, the energetically preferred crystal structures for the three side-chain orientations do not fit with the observed patterns due to the absence of the 2 mm symmetry for the 0*kl* lattice, as expected. Furthermore, the strong 100 reflection is absent from the simulation, both for electron diffraction and X-ray powder diffraction. $P2_1(a)$ was therefore eliminated for the three side-chain models (trans, g^+, and g^-). The $P2(c)$ and $P2_1(c)$ space groups also lacked, as expected, the 2 mm symmetry along the a^* and b^* axes of the *hk*0 reciprocal lattice. Moreover, if α is fixed at 90°, the packing is unstable, as demonstrated by the resulting positive packing energy. For the $P2(c)$ space group, the intense 001 peaks are not present in the observed data but show up in the simulated X-ray powder diffraction profiles for the three side-chain models. For the $P2_1(c)$ space group, the existence of a relatively strong 001 or 010 peak for the two gauche side chains and a relatively strong peak at $2\theta = 21°$ for the trans side-chain in the X-ray powder diffraction profiles led to its exclusion for the three side chain models. For all these reasons, the $P2(c)$ and $P2_1(c)$ space groups were not considered any further.

For the $P2_1(b)$ space group, only the trans model gives a reasonable fit with experimental intensities. The two gauche models yield a too weak calculated intensity for the 200 peak and a too strong intensity for the 120 peak. In addition, the 020 spots are too weak and the 010 peaks too intense in the simulated electron diffraction patterns in comparison with the observation. Energetically, the two gauche models yield similar packing energies to those for the trans model, but after flexible optimization, the g^- model changes from a planar zigzag conformation to a helical conformation and the g^+ model results in a much higher packing energy. Chain rotation and translation do not yield a better fit with the experimental data, and therefore, these two possibilities were eliminated.

Comparison between the Two-Step and Single-Step Approaches. The previous calculations led us to retain the $P2_1$ space group with a unique *b* axis and a trans side chain. Two chains are packed antiparallel in a monoclinic lattice. The rigid model packed in the $P2_1(b)$ space group is designated by the subscript r, while the structure simultaneously minimized for both intra- and intermolecular interactions is designated as the flexible model by the subscript f. A comparison with X-ray data appears in Table 2. Again, the densities calculated from the unit cells are acceptable in comparison with the observed value of 1.10 g/cm^3.

In Figure 3, the experimental X-ray powder diffraction spectrum[10] (curve a), after removing the amorphous halo, is compared to those simulated for the rigid and flexible models (curves b and c, respectively); the diffraction angles 2θ, *d* spacings, and relative intensities of the stronger reflections are listed in Table 2. The orthorhombic unit cell[11] previously proposed is also included in this table. All cell parameters are kept as in ref 11 except for the fiber period and the β angle. The simulation models yield a smaller β angle (~83°) than the orthorhombic crystal lattice.[11] For the rigid model, *c* is chosen to be equal to the fiber period of the minimized conformation of the isolated chain whereas β is determined from an intermolecular interaction optimization. For the flexible model, both *c* and β are produced from a simultaneous intermolecular and intramolecular interaction optimization. For practical reasons, *c* was not constrained to the experimental value during the energy minimization.

The positions of the observed strong reflections are in good agreement with those of the proposed orthorhombic unit cell and with those of the monoclinic unit cells derived from the simulations (see Table 2). The most important difference occurs for the assignment of the 120 and 210 reflections, which is inverted in the simulated models and the orthorhombic unit cell.

As can be seen in Figure 3, the relative intensity and the shape of the stronger reflections at the 2θ diffraction angles 15.43, 19.64, 23.03, 23.92, 25.90, 28.13, 31.27, and 37.61° for both the rigid and flexible models are very similar to those observed, except for the 100 peak, which has a stronger intensity in the flexible model in comparison to the experimental curve. For the two energy-minimized models, *R* factors were calculated using structural factors reported in Table 3 for 12 observed reflections. The thermal factor was optimized in the range 0−25 Å^2 in order to yield the lowest *R* factor. The

Table 2. Diffraction Angles 2θ, Bragg Distances d, and Relative Intensities I of the Reflections Observed[10,11] and Calculated for the $P2_1(b)$ trans Side-chain Model[a]

	exp[10]		orthorhombic unit cell[11]		rigid model			flexible model		
hkl	d_o (Å)	I_o	d (Å)	2θ (deg)	d_{cr} (Å)	$2\theta_{cr}$ (deg)	I_{cr}	d_{cf} (Å)	$2\theta_{cf}$ (deg)	I_{cf}
100	9.06	27	9.09	9.73	9.04	9.79	27	9.03	9.79	40
110	5.73	100	5.79	15.30	5.74	15.43	100	5.74	15.43	100
200	4.54	8	4.55	19.51	4.52	19.64	11	4.52	19.65	11
10$\bar{1}$	3.96	10	4.21	21.10	4.06	21.87	21	4.05	21.96	20
011			4.00	22.22	4.05	21.97		4.04	22.01	
210	3.86	13	3.90	22.80	3.86	23.03	14	3.86	23.03	15
020	3.74	10	3.77	23.60	3.72	23.92	13	3.72	23.92	14
120	3.53	16	3.49	25.52	3.44	25.90	23	3.44	25.90	23
201			3.25	27.44	3.51	25.40		3.51	25.39	
211	3.17	2	3.00	29.72	3.17	28.13	3	3.17	28.12	2
021			2.91	30.72	2.95	30.35		2.94	30.38	
220	2.84	6	2.91	30.72	2.87	31.14	10	2.87	31.15	9
121			2.79	32.11	2.86	31.27		2.86	31.28	
311	2.56	1	2.43	36.99	2.54	35.37	1	2.54	35.24	1
130		5	2.43	36.99	2.39	37.61	8	2.39	37.61	7
002	2.38	2	2.36	38.13	2.41	37.29	4	2.40	37.41	3
320		2	2.36	38.13	2.34	38.45	4	2.34	38.46	3
102			2.28	39.52	2.40	37.47		2.40	37.55	
400			2.28	39.52	2.26	39.90		2.26	39.92	
012			2.28	39.52	2.29	39.28		2.29	39.39	
230			2.18	41.42	2.17	41.54		2.17	41.54	
410		4	2.18	41.42	2.16	41.78	7	2.16	41.80	6
cell parameters			a = 9.10 Å, b = 7.44 Å, c = 4.75 Å; $\alpha = \beta = \gamma = 90°$		a = 9.10 Å, b = 7.44 Å, c = 4.48 Å $\alpha = \gamma = 90°$, $\beta = 83.34°$			a = 9.10 Å, b = 7.44 Å, c = 4.84 Å; $\alpha = \gamma = 90°$, $\beta = 83.12°$		
densities (g/cm^3)	1.10		1.180		1.161			1.165		

[a] Relative intensities correspond to the maxima of Figure 3. The subscript c refers to calculated, and the subscript o refers to observed values; r refers to the rigid model, and f, to the flexible model.

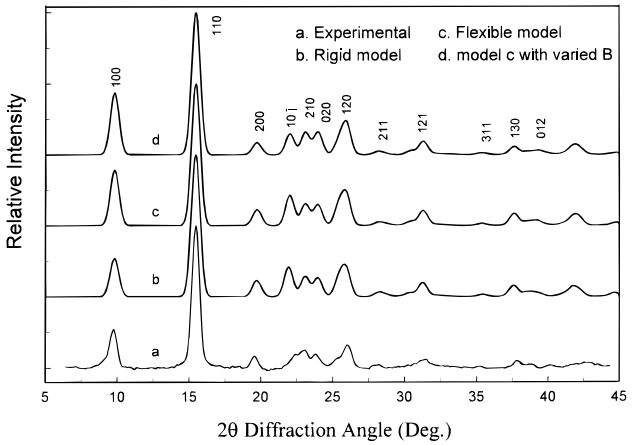

Figure 3. X-ray powder diffraction profiles of melt-crystallized isotactic PMEPL: (a) experimental spectrum[10] after subtraction of the amorphous halo; (b) simulated spectrum for the rigid model (B = 3.0 Å^2 for all atoms); (c) simulated spectrum for the flexible model (B = 3.0 Å^2 for all atoms); (d) simulated spectrum for the flexible model using the isotropic thermal factor B = 25 Å^2 for atoms of the ethyl group and B = 3.0 Å^2 for all other atoms.

thermal factor 3.0 Å^2 (for all atoms) gives the lowest R factors, 0.16 and 0.20 for the flexible and rigid models, respectively. These values are surprisingly good when taking into account that they were obtained for energy-minimized models and that the atom and chain positions were never minimized with X-ray and electron diffraction data. Refining against these data would undoubtedly lead to an even lower value of R, without changing the final structure in any major way.

The electron diffraction patterns simulated for the $hk0$ and $0kl$ reciprocal lattices are shown in Figures 4 and 5, respectively. Both patterns have a 2 mm symmetry. The 110, 100, 200, 020, 120, 130, 210, 220, 320, 230, 040, 012, and 002 reflections are clearly observed in the electron diffraction pattern. It must be noted that the medium-to-weak-intensity 040 reflection is outside the range studied in the X-ray diffraction pattern and is, therefore, observed in the electron diffraction pattern only. No significant difference is found in Figures 4 and 5 between the rigid and flexible models.

Table 3. Observed (F_o) and Calculated (F_c) X-ray Powder Diffraction Structure Factors for the Rigid and Flexible Models (B = 3.0 Å^2 for all atoms)

		rigid model			flexible model		
indices			F_c			F_c	
hkl	m_i	F_o	individual	merged	F_o	individual	merged
100	2	1125.2	535.7	535.7	1052.7	730.7	730.7
110	4	3540.8	3540.8	3540.8	3312.8	3312.8	3312.8
200	2	1161.7	533.9	786.3	1086.9	489.7	726.9
101	2	1161.7	155.1	786.3	1086.9	156.1	726.9
10$\bar{1}$	2	1960.4	1275.9	1821.2	1834.1	1224.1	1748.5
011	4	1960.4	123.3	1821.2	1834.1	123.0	1748.5
210	4	1588.1	552.4	1105.6	1485.9	559.0	1119.2
111	4	1588.1	21.0	1105.6	1485.9	26.1	1119.2
020	2	2127.9	1622.8	1622.8	1990.8	1708.0	1708.0
201	2	1791.4	1822.9	1822.9	1676.1	1854.9	1854.9
120	4	2296.1	1886.0	1886.0	2148.3	2017.8	2017.8
211	4	755.0	164.3	430.1	706.4	137.8	365.9
20$\bar{1}$	2	755.0	196.2	430.1	706.4	170.2	365.9
300	2	1946.8	91.7	1165.7	1821.5	75.3	1186.2
021	4	1946.8	189.7	1165.7	1821.5	204.1	1186.2
21$\bar{1}$	4	1946.8	43.5	1165.7	1821.5	41.7	1186.2
220	4	1946.8	275.3	1165.7	1821.5	257.7	1186.2
121	4	1946.8	465.3	1165.7	1821.5	483.2	1186.2
310	4	1946.8	62.6	1165.7	1821.5	60.4	1186.2
12$\bar{1}$	4	1946.8	50.8	1165.7	1821.5	44.6	1186.2
311	4	315.0	278.4	278.4	294.8	272.8	272.8
002	2	2149.2	291.9	1667.5	2010.8	302.2	1648.1
102	2	2149.2	378.5	1667.5	2010.8	363.9	1648.1
130	4	2149.2	604.3	1667.5	2010.8	590.8	1648.1
320	4	2149.2	341.3	1667.5	2010.8	300.2	1648.1
31$\bar{1}$	4	2149.2	290.85	1667.5	2010.8	339.0	1648.1
012	4	2149.2	64.9	1667.5	2010.8	58.7	1648.1
112	4	2149.2	101.9	1667.5	2010.8	98.4	1648.1

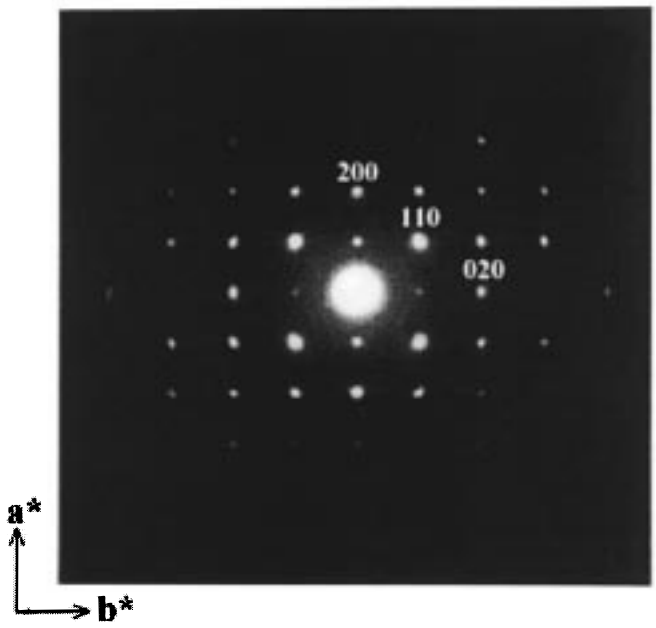

(a). Experimental

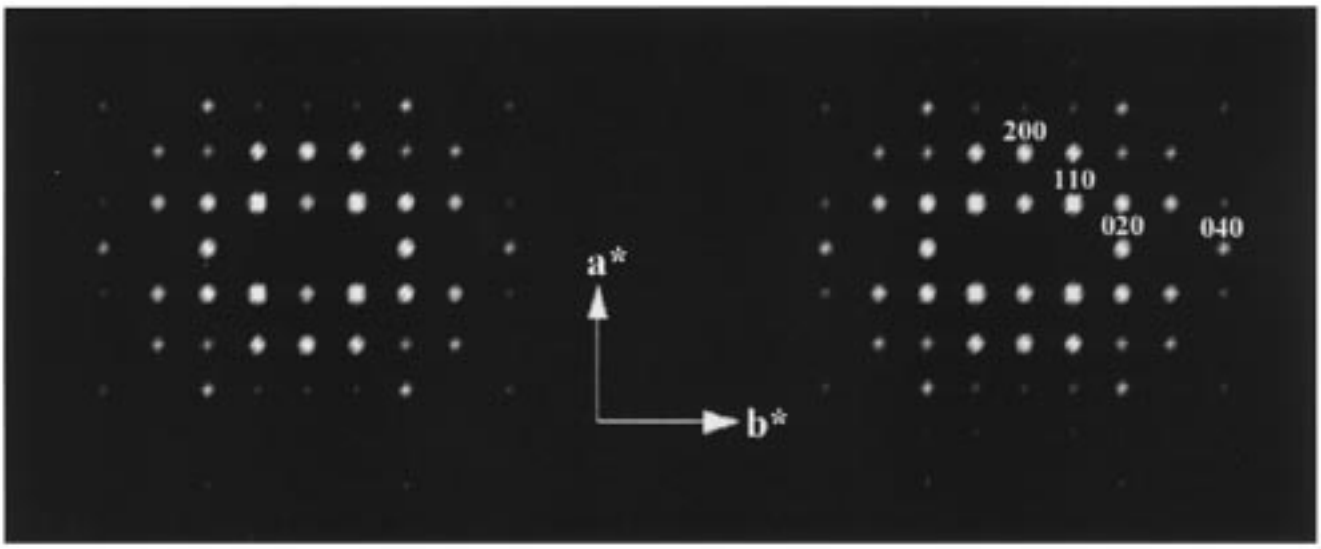

(b). Rigid Model (c). Flexible Model

Figure 4. *hk*0 electron diffraction patterns (a*, vertical; b*, horizontal): (a) experimental;[11] (b) calculated for the rigid model; (c) calculated for the flexible model.

The major difference between the simulated and experimental electron diffraction spectra is the absence of the weak 010 and 030 reflections in the simulated patterns due to the systematic absence of 0*k*0 ($k = 2n + 1$) reflections of the $P2_1(b)$ space group. It has been proposed,[11] on the basis of the electron diffraction patterns, that no systematic absence occurred on the *hk*0, 0*kl*, *h*00, 00*l*, and 0*k*0 planes. The systematic presence of *hk*0, 0*kl*, and *h*00 planes is confirmed by X-ray diffraction where the 001, 003, 010, and 030 reflections cannot be unambiguously identified at the 2θ diffraction angles 18.46, 57.55, 11.90, and 36.22°, respectively. The presence of 0*k*0 reflections with odd *k* in the electron diffraction spectrum could be due to multiple scattering.[11] Another possibility for the presence of 010 and 030 spots could be a distortion of the packing symmetry. For the flexible model, if only one of the two chains in the unit cell is rotated along the *c* axis by an angle on the order of 20°, instead of both chains as symmetry would require, while all the other cell parameters and internal coordinates are kept fixed, the simulated electron diffraction pattern displays 010 and 030 spots. In such a case, the symmetry could probably be reduced to *P*1. This artificial packing structure is energetically allowed with a packing energy of −20.63 kcal·mol^{-1} per repeat unit as compared to −15.9 kcal·mol^{-1} per repeat unit for the rigid model but does not correspond to a packing energy minimum.

It is obvious from Figure 3 that the two models show a more intense $10\bar{1}$ reflection than that observed in the

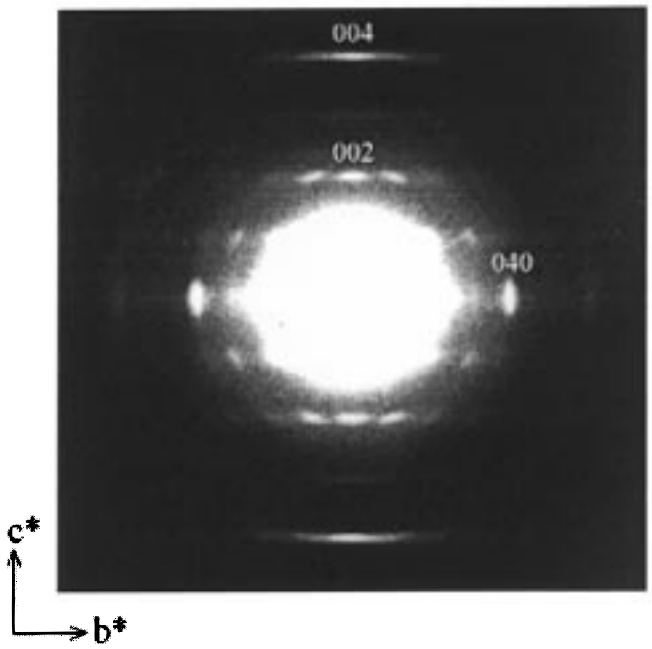

(a). Experimental

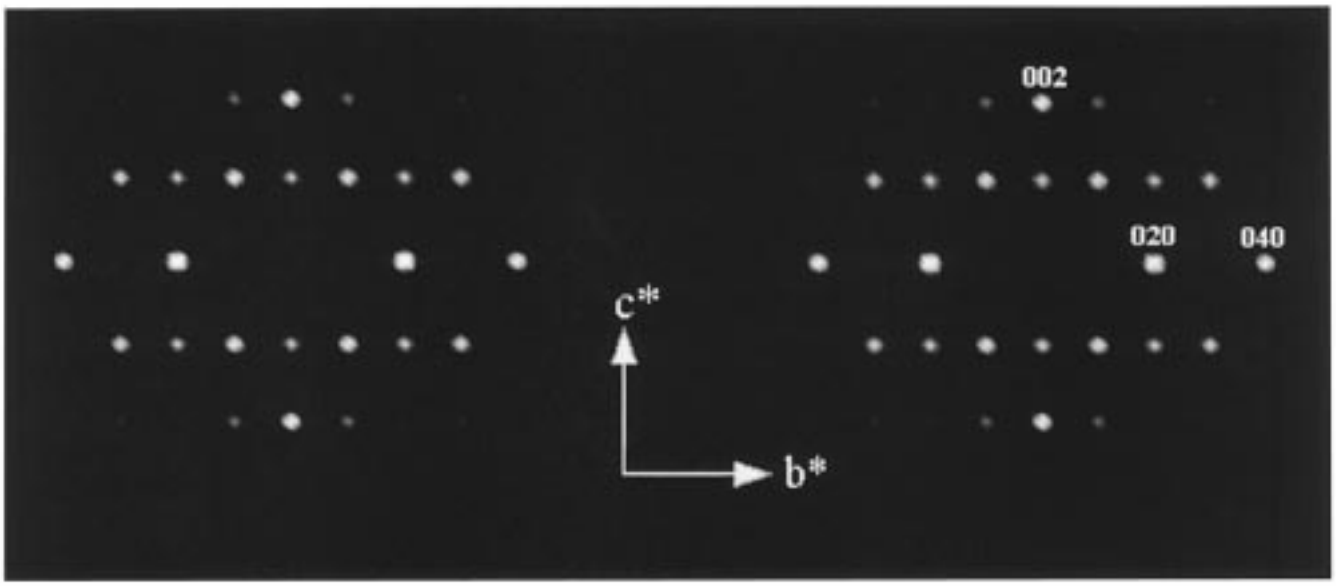

(b). Rigid Model (c). Flexible Model

Figure 5. 0*kl* electron diffraction patterns (c*, vertical, b*, horizontal): (a) experimental;[11] (b) calculated for the rigid model; and (c) calculated for the flexible model.

X-ray diffraction profile. A distortion of the side-chain dihedral angles could reduce the relative $10\bar{1}$ intensity. Keeping this in mind, the X-ray powder diffraction pattern was resimulated for the flexible model using the isotropic thermal factor $B = 25$ Å^2 for all atoms of the ethyl groups while the other atoms were kept at the initial value = 3.0 Å^2. These values of thermal factor yielded a higher but still acceptable R factor of 0.23. The resulting curve is illustrated in Figure 3d, and from the comparison between curves c and d, it is concluded that a high thermal factor greatly decreases the relative intensity of several strong reflections, such as 100, 200, 121, and 130, especially that of $10\bar{1}$, and that the model is in better agreement with the data. It is therefore proposed that some disorder is present in the lateral chain packing, which is simulated in this calculation with an increase in the isotropic thermal factor. The disorder in lateral chain packing could be a symptom of symmetry break in the short range; because of the small ratio of data to refinement variables and because of the intrinsic width of reflections observed in X-rays, we did not feel justified to lower the symmetry.

In Table 4, observed (F_o) and calculated (F_c) structure factors of the major $hk0$ reflections observed in electron diffraction are given for both the rigid and flexible models. The use of a B factor of 4.0 Å^2 led to the lowest and reasonable R factor, 0.20 for the flexible model and 0.23 for the rigid model for 14 diffraction spots. The

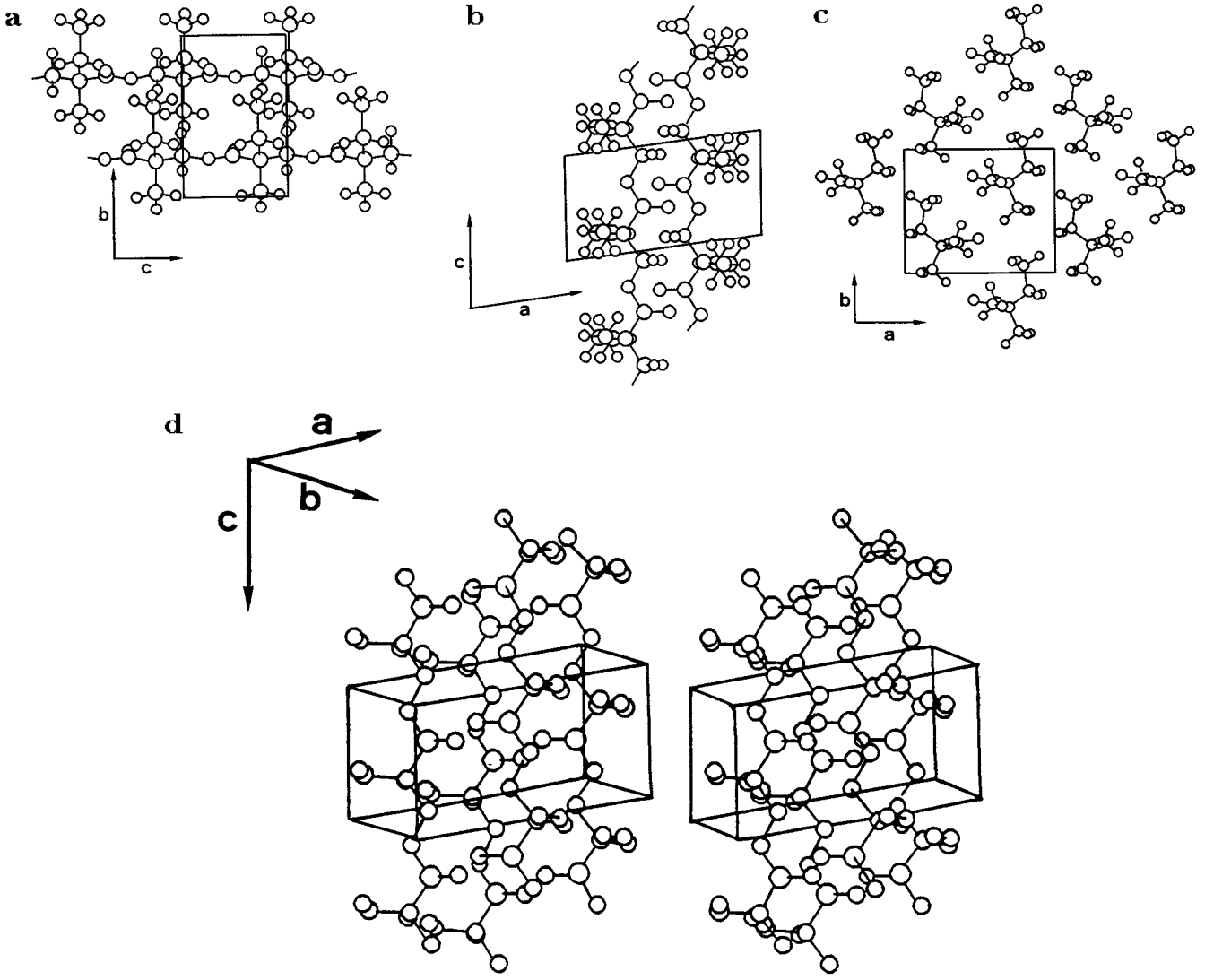

Figure 6. Monoclinic packing for the flexible model: (a) projection along the *a* axis; (b) projection along the *b* axis; (c) projection along the *c* axis; (d) stereodrawing.

Table 4. Observed (F_o) and Calculated (F_c) Electron Diffraction Structure Factors for the Rigid and Flexible Models (B = 4.0 Å^2 for All Atoms)

		flexible model		rigid model	
hkl	d_c (Å)	F_c	F_o	F_c	F_o
100	9.03	37.1	116.8	23.0	100.7
010	7.44	0.0	47.7	0.0	41.1
110	5.74	219.0	214.6	224.3	184.9
200	4.52	92.2	135.5	93.8	116.8
210	3.86	76.2	107.8	68.8	92.9
020	3.72	106.0	119.1	94.2	102.6
120	3.44	109.8	109.8	94.6	94.6
300	3.01	11.0	21.6	10.9	18.6
220	2.87	31.65	55.6	27.5	47.9
310	2.79	14.4	17.7	11.8	15.3
130	2.39	74.4	71.5	63.6	61.6
320	2.34	44.9	41.1	43.4	35.4
230	2.17	42.8	42.6	37.3	36.7
040	1.86	54.8	39.5	34.6	34.1

evaluation of the *R* factor was not done for 0*kl* reflections because of uncertainties in the intensity related to the width of the 0*kl* diffraction spots.

In Figure 6, the packing of the flexible model is shown; the antiparallel packing in the $P2_1(b)$ space group can be clearly identified. The shortest distance between two nonbonded atoms is 2.36 Å for a H...H pair. From an intramolecular interaction point of view, the dipole moment vectors are parallel along a single planar zigzag chain. The total intramolecular energy and various energy contributions of the flexible model are almost the same as those of the original conformation, as shown in Table 5. This similarity indicates that the conformation is very similar before and after flexible minimization. In fact, it can be seen in Table 6 that there is no significant difference between the geometries of the two models. Intermolecularly, both the rigid and flexible models lead to reasonable negative packing energies, while the latter has a lower value (−26.64 kcal·mol^{-1} per repeat unit) than the former (−15.87 kcal·mol^{-1} per repeat unit). Among the various intermolecular interactions, the nonbonded atomic van der Waals interactions, that is, repulsion and dispersion energies, are almost unchanged, as shown in Table 5. The antiparallel packing is mainly favored by van der Waals interactions (about −21 kcal·mol^{-1} per repeat unit). This conclusion is also in agreement with the proposed structures of α- and γ-polypivalolactones, where Coulombic interactions are far less important than nonbonded van der Waals interactions.[6] After the full-relaxation optimization of the chains, the flexible model is slightly distorted as compared to the rigid

Table 5. Interaction Energies (in kcal·mol^{-1} per Repeat Unit) for the Rigid and Flexible Models

	intramolecular				intermolecular			
	$E_{repulsion}$	$E_{dispersion}$	$E_{Coulombic}$	E_{intra}	$E_{repulsion}$	$E_{dispersion}$	$E_{Coulombic}$	$E_{packing}$
two-helix model	88.4	−76.3	27.8	39.9				
rigid model	88.4	−76.3	27.8	39.9	21.1	−42.7	5.7	−15.9
flexible model	89.2	−76.8	27.9	40.3	21.4	−43.4	−4.7	−26.6

Table 6. Geometrical Features of Simulated PMEPL Crystal Structures for the Rigid and Flexible Models Packed in the $P2_1(b)$ Space Group

internal coordination	rigid	flexible
Bond Lengths (Å)		
C(1)−C(2)	1.538	1.535
C(2)−C(3)	1.541	1.540
C(3)−O(1)	1.363	1.361
O(1)−C′(1)	1.428	1.425
C(3)−O(2)	1.203	1.205
C(2)−C(4)	1.554	1.553
C(2)−C(5)	1.560	1.560
C(5)−C(6)	1.534	1.533
Bond Angles (deg)		
C′(1)−O(1)−C(3)	117.3	117.1
O(1)−C(3)−C(2)	112.5	112.1
O(2)−C(3)−C(2)	125.1	125.3
O(1)−C(3)−O(2)	122.4	122.6
C(1)−C(2)−C(3)	106.8	106.6
C(1)−C(2)−C(4)	111.2	111.2
C(1)−C(2)−C(5)	113.5	113.5
C(3)−C(2)−C(4)	108.4	108.2
C(3)−C(2)−C(5)	109.2	109.9
C(4)−C(2)−C(5)	107.6	107.4
C(2)−C(5)−C(6)	117.4	117.5
O′(1)−C(1)−C(2)	111.5	111.6
Torsion Angles (deg)		
τ, C(2)−C(3)−O(1)−C′(1)	−180	−179
ψ, C(3)−O(1)−C′(1)−C′(2)	180	178
η, O″(1)−C(1)−C(2)−C(3)	179	−180
ϕ, C(1)−C(2)−C(3)−O(1)	179	−177
χ, C(4)−C(2)−C(5)−C(6)	−176	−178

Table 7. Fractional Coordinates of the Final Model Obtained with the Flexible Approach

atom	*x*	*y*	*z*
C1	0.395 44	0.240 48	−0.089 06
H1−C1	0.443 03	0.103 80	−0.096 95
H2−C1	0.488 24	0.337 27	−0.108 54
C2	0.295 69	0.271 49	0.185 76
C4	0.234 31	0.466 44	0.204 48
H1−C4	0.164 47	0.491 49	0.402 87
H2−C4	0.323 46	0.567 42	0.182 75
H3−C4	0.165 69	0.489 66	0.034 91
C5	0.160 47	0.141 47	0.229 06
H1−C5	0.091 12	0.169 14	0.061 17
H2−C5	0.090 73	0.176 42	0.424 59
C6	0.192 60	−0.060 75	0.229 58
H1−C6	0.088 11	−0.136 91	0.263 40
H2−C6	0.251 99	−0.105 71	0.029 69
H3−C6	0.259 31	−0.098 74	0.396 08
C3	0.393 80	0.245 22	0.420 75
O2	0.524 71	0.213 91	0.387 69
O1	0.315 61	0.261 99	0.677 41

model, as the internal geometry is readjusted in order to decrease the packing energy. Slight differences can be noted for the torsion angles given in Table 6: η is closer to 180° than in the rigid model, and this tendency is analogous to the results for PPL[6] from the single-step procedure. The major difference between packing energies in the rigid and flexible models stems from the Coulombic interactions, which changed from 5.7 to −4.7 kcal·mol^{-1} per repeat unit after the flexible energy minimization.

It should be stressed, however, that the packing energy is not the most important criterion to judge if the packing is reasonable. Comparison with X-ray and electron diffraction patterns through structure factor calculations is the ultimate proof that a structure does exist. For instance, in the present study, $P2(c)$ and $P2_1(c)$ space groups yield crystal structures with lower packing energies (−43.2 kcal·mol^{-1} per repeat unit for the former and −40.0 kcal·mol^{-1} per repeat unit for the latter) than that of the $P2_1(b)$ space group, but their resulting diffraction patterns are not compatible with the observation.

Finally, the fractional coordinates of one asymmetric unit for the flexible model are reported in Table 7.

Conclusions

The melt-crystallized structure of isotactic PMEPL has been determined on the basis, on one hand, of conformational energy and packing energy calculations and on the other hand, of X-ray and electron diffraction data. Two extended planar zigzag backbone chains with trans side chains, corresponding to the lowest energy minimum of an isolated chain, were packed antiparallel in the $P2_1(b)$ space group. Both the two-step and single-step procedures were used to optimize the crystal structure. Considerations of the density, fiber period, packing energy, electron diffraction patterns, X-ray powder diffraction profiles, and structure factor calculations for the rigid and flexible models demonstrate that the two procedures yield similar results, in fairly good agreement with the observations. However, the flexible model shows a lower packing energy and a lower discrepancy factor than the rigid model.

Acknowledgment. The authors acknowledge the National Sciences and Engineering Research Council of Canada and the Department of Education of the Province of Quebec (FCAR program) for financial support. Z.H. also expresses his thanks to Dr. Anna M. Ritcey and Mr. Claude-Paul Lafrance for useful discussions. We finally thank Dany Bussières (Département de Biologie, Université Laval) for his help in image analysis.

References and Notes

(1) Tadokoro, H. *Structure of Crystalline Polymers*; Robert E. Krieger Pub. Co.: Malabar, 1990.
(2) Tripathy, S. K.; Hopfinger, A. J.; Taylor, P. L. *J. Phys. Chem.* **1981**, *85*, 1371.
(3) McCullough, R. L. *J. Macromol. Sci. Phys.* **1974**, *9*, 97.
(4) Sorensen, R. A.; Liau, W. B.; Boyd, R. H. *Macromolecules* **1988**, *21*, 194.
(5) Liau, W. B.; Boyd, R. H. *Macromolecules* **1990**, *23*, 1531.
(6) Ferro, R.; Bruckner, S.; Meille, S. V.; Ragazzi, M. *Macromolecules* **1990**, *23*, 1676.
(7) Boyd, R. H. *Adv. Polym. Sci.* **1994**, *116*, 1.
(8) Wunderlich, B. *Macromolecular Physics, Vol. 1. Crystal Structure, Morphology, Defects*; Academic Press: New York, 1973.
(9) Discover, Polymer and Insight II User Guides, version 3.0.0, Biosym/MSI, San Diego, 1995.

(10) Ritcey, A. M.; Prud′homme, R. E. *Macromolecules* **1992**, *25*, 972.
(11) Ritcey, A. M.; Brisson, J.; Prud′homme, R. E. *Macromolecules* **1992**, *25*, 2705.
(12) Prud′homme, R. E.; Ritcey, A. M. *Makromol. Chem., Macromol. Symp.* **1993**, *73*, 203.
(13) Ritcey, A. M.; Prud′homme, R. E. *Macromolecules* **1993**, *26*, 1376.
(14) Sun, H.; Mumty, S. J.; Maple, J. R.; Hagler, A. T. *J. Am. Chem. Soc.* **1994**, *116*, 2978.
(15) Sun, H. *J. Comput. Chem.* **1994**, *15*, 752.
(16) Rosa, C. D.; Borriello, A.; Corradini, P. *Macromolecules* **1996**, *29*, 6323.
(17) Dorset, D. L. *J. Electron Microsc. Tech.* **1985**, *2*, 89.

MA980830L